Journal of Nuclear Materials 491 (2017) 199–205

Contents lists available at ScienceDirect

Journal of Nuclear Materials

journal homepage: www.elsevier.com/locate/jnucmat

The effect of low energy helium ion irradiation on tungsten-tantalum (W-Ta) alloys under fusion relevant conditions

S. Gonderman*, J.K. Tripathi, T.J. Novakowski, T. Sizyuk, A. Hassanein

Center for Materials Under Extreme Environment (CMUXE), School of Nuclear Engineering Purdue University, West Lafayette, IN 47907, USA

ARTICLE INFO

Article history:
Received 10 December 2016
Received in revised form
10 May 2017
Accepted 10 May 2017
Available online 11 May 2017

Keywords:
Fusion
Fuzz
Tungsten
Irradiation resistant
Alloys
Helium
Low energy

ABSTRACT

Currently, tungsten remains the best candidate for plasma-facing components (PFCs) for future fusion devices because of its high melting point, low erosion, and strong mechanical properties. However, continued investigation has shown tungsten to undergo severe morphology changes under fusion-like conditions. These results motivate the study of innovative PFC materials which are resistant to surface morphology evolution. The goal of this work is to examine tungsten-tantalum (W-Ta) alloys, a potential PFC material, and their response to low energy helium ion irradiation. Specifically, W-Ta samples are exposed to 100 eV helium irradiations with a flux of 1.15×10^{21} ions m^{-2} s^{-1}, at 873 K, 1023 K, and 1173 K for 1 h duration. Scanning electron microscopy (SEM) reveals significant changes in surface deterioration due to helium ion irradiation as a function of both temperature and tantalum concentration in W-Ta samples. X-Ray Diffraction (XRD) studies show a slight lattice parameter expansion in W-Ta alloy samples compared to pure W samples. The observed lattice parameter expansion in W-Ta alloy samples (proportional to increasing Ta wt.% concentrations) reflect significant differences observed in the evolution of surface morphology, i.e., fuzz development processes for both increasing Ta wt.% concentration and target temperature. These results suggest a correlation between the observed morphology differences and the induced crystal structure change caused by the presence of tantalum. Shifts in the XRD peaks before and after 100 eV helium irradiation with a flux of 1.15×10^{21} ions m^{-2} s^{-1}, 1023 K, for 1 h showed a significant difference in the magnitude of the shift. This has suggested a possible link between the atomic spacing of the material and the accumulated damage. Ongoing research is needed on W-Ta alloys and other innovative materials for their application as irradiation resistant materials in future fusion or irradiation environments.

1. Introduction

Tungsten remains one of the primary materials for plasma-facing components (PFCs) in future fusion devices, *viz.*, ITER and DEMO (DEMOnstration Power Station). This is due to tungsten's good thermomechanical properties, low erosion, and limited tritium retention [1–3]. It has the highest melting point of all metals (~3410 °C) and has good thermal conductivity [3]. Additionally, it has a high threshold for physical sputtering of ~200 eV [1]. Finally, it does not form hydrides or co-deposits with tritium (T) which results in less tritium retention when compared to carbon based PFC [1,4,5]. Despite these inherent advantages recent research on tungsten (W) as PFC material has shown tungsten to undergo severe surface morphology evolution in response to low energy (~100 eV) helium (He) and deuterium (D) irradiation. Mechanisms leading to the formation of bubbles [6–8], blister [9–11], and eventually fuzz [12–14] are still being investigated. Furthermore, the effects of these extreme morphologies on device operation and plasma performance are uncertain. These issues regarding W as PFC prompt the need for investigation of alternative wall materials in order to better understand the fundamental mechanisms and physics behind this extreme morphology evolution and to develop materials better suited to harsh fusion environments.

Tungsten alloys have sparked some interest as a potential PFC material. The alloying of tungsten with certain materials like rhenium (Rh) has been shown to improve ductility [15,16]. Other alloys, such as oxide dispersion strengthened (ODS) heavy alloys, have been shown to exhibit enhanced mechanical properties [17,18]

* Corresponding author.
E-mail address: sgonderm@purdue.edu (S. Gonderman).

http://dx.doi.org/10.1016/j.jnucmat.2017.05.009
0022-3115/

and even reduced hardening and embrittlement when exposed to high energy neutron irradiation [19,20]. This result has motivated study of additional W alloys such as W-Ta alloy materials. Recent work [21] investigated the mechanical properties of W-Ta alloys and showed that the alloying of W with Ta does not have the same ductility enhancement as compared to that of the W-Rh. Additionally, they also observed that the toughness for crack propagation may be enhanced for carefully designed PFC W-Ta alloy materials [21]. Other studies on W-Ta alloys have shown increased hardness as a function of neutron damage simulated by ion implantation [22]. Further, research on W-Ta alloy's response to thermal shock *via* transient heat loading has shown a significant improvement when compared to pure W materials [23,24]. Perhaps that most significant enhancement, of W-Ta alloys, for fusion applications may be in regards to retention of hydrogen (H) isotopes. Several recent studies [25–27] have looked exclusively at these issues. Results suggest that W-Ta alloys exhibit significantly reduced D retention under fusion relevant conditions. These advantages suggest W-Ta alloys may be considered as possible alternative PFC material for current and future DEMO reactors.

Despite the extensive work on testing the mechanical properties of W-Ta alloys, very little effort has been done on understanding the surface modification of W-Ta alloys when exposed to fusion relevant He ion fluxes in fusion environment. The work presented here focuses on the surface morphology evolution driven by low energy He^+ ion irradiation of W and W-Ta alloys. Specifically, pure W and W-Ta alloys of 1, 3, and 5 wt.% Ta are exposed to low energy He^+ ion irradiation at various temperatures. Post irradiation characterization using SEM revealed significant surface morphology dependence on both Ta concentration and temperature. Further analysis using XRD linked this behavior with slight crystallographic change induced by the alloying process.

2. Materials and experimental methods

The experimental work detailed here uses four different W based materials: one 99.95% pure W (from Alfa Aesar), and three W-Ta alloys having 1, 3, and 5 wt.% of Ta (from American Elements). High resolution SEM of pristine samples confirmed homogeneous distribution of Ta throughout the sample. When referring to these samples going forward the following name convention will be used: W, W-1Ta, W-3Ta, and W-5Ta corresponding to pure W and, 1, 3, and 5 wt.% of Ta, respectively.

In order to verify the composition of the W-Ta alloy materials *in-situ*, pre-irradiation X-ray photoelectron microscopy (XPS) characterization was performed in the Interaction of Materials with Particles and Components Testing experimental (IMPACT) [28] chamber at Center for Materials Under eXtreme Environment (CMUXE), Purdue University. The XPS results confirmed the Ta concentrations of the W-Ta alloy materials to within 0.3% uncertainty of that reported from the commercial companies. Samples undergoing XPS were sputter cleaned with 1 keV Ar^+ ions to remove oxygen and surface impurities (e.g., carbon) in order to achieve accurate alloy compositional information.

Samples of the W, W-1Ta, W-3Ta, and W-5Ta were cut from large sheets into 10 mm × 10 mm × 2 mm samples. 16 total W and W-Ta samples (4-W, 4-W-1Ta, 4-W-3Ta, and 4-W-5Ta samples) were mechanically polished to a mirror finish prior to He^+ ion irradiation. He^+ ion exposures were conducted in the ultra-high flux irradiation laboratory (UHFI-II) at CMUXE [29]. One of each sample type was cleaned using 1 keV Ar^+ ion irradiation for XPS compositional analysis and 12 of the samples (3-pure W, 3 -1% Ta, 3-3% Ta, and 3–5% Ta) were exposed to 100 eV He^+ ion irradiation with a flux of 1.15×10^{21} ions m^{-2} s^{-1}, at 873, 1023, and 1173 K for 1 h durations in each case. The temperature threshold for fuzz formation in W has been shown to be > 1000 K [12]. Therefore in the present work, three temperatures all near this threshold were selected in order to investigate the temperature effect of the fuzz formation process. Fig. 1 shows a schematic of the experimental setup used during these irradiation experiments.

Surface morphology changes were monitored with field emission (FE) scanning electron microscopy (SEM), using Hitachi S-4800 Field Emission SEM. For the XPS measurements, photoelectrons were excited by an Mg-Kα (energy = 1253.6 eV) X-ray radiation source (SPECS XRC-1000), and the emitted photoelectrons were analyzed with Omicron Argus hemispherical electron analyzer using a round aperture of 0.63 mm (for imaging-XPS) and a second aperture at 6.3 mm (for conventional XPS). No sample charging was observed. All XPS spectra were analyzed with commercial CasaXPS software [30]. Crystalline phase analyses were performed with X-ray diffraction using Bruker D8 Focus X-Ray Diffractometer. Optical reflectivity measurements [29] were performed over a spectrum of incident light wavelength (λ) ranging from 200 to 1100 nm (using a combination of halogen and deuterium light source and a beam diameter of ~1 mm). Maya 2000 Pro Spectrometer from Ocean Optics was used for signal detection. Before the reflectivity measurements began, the spectrometer was calibrated using Spectralon white reference plate having 100% reflectivity. The observed reflection in our system is mainly specular. A specular reflection is a reflection of a mirror like surface (keeping in mind that different surfaces to different wavelengths may or may not be mirror like). Specular reflection will result when the surface roughness is smaller than the applied wavelength of light (and diffuse reflection will result when the surface roughness is larger than the wavelength). A specular reflectance of 100% would correspond to an ideal mirror, typical specular reflectance are less than the maximum value (*i.e.*, 100%). For collecting the reflected light a "*reflection probe*" from Ocean Optics was used which can collect light at the same angle as it illuminates, and can be used for either specular or diffuse reflection measurements. In fact it is made of 6 illumination fibers around a single read fiber (in the center), which results in a 25° full angle field of view. Each illumination fiber projects a cone of light from the source and all of them overlap at the sample in the center, exactly where the central read fiber is situated. Thus, in principle the reflectivity for an ideal mirror will be ~100%. During our measurements the "*reflection probe*" was placed at 90° to the sample surface (along the sample surface normal). The distance between sample and "*reflection probe*" was ~1 mm.

3. Results and discussion

3.1. Field emission (FE) scanning electron microscopy (SEM) studies

Fig. 2 (a) - (d) is a set of SEM images for four W-Ta alloy samples (W, W-1Ta, W-3Ta, and W-5Ta). In each case samples were exposed to 100 eV He^+ ions at 873 K. There is slight variation in the surface morphology for the different samples as a function of Ta concentration. All the surfaces display roughening with notable reduction in observed feature size as Ta concentration is increased. Specifically, there are small pores present in all the images and the largest of these pores are clearly evident in Fig. 2(a) which is the pure W sample. In addition to the pore sizes, the surface appears to be less damaged in the W-Ta samples.

Fig. 2(e)–(h) is another set of four SEM images for four W-Ta alloy samples (W, W-1Ta, W-3Ta, and W-5Ta). As of the previous cases here also samples were exposed to low energy He^+ ions but at 1023 K. Note, although the target temperature difference between the previous set of experiments (Fig. 2 (a) -(d)) and the present one (Fig. 2(e)-(h)) is only 150 K, the difference in surface morphology is significant, leading to very clear surface morphology dependence

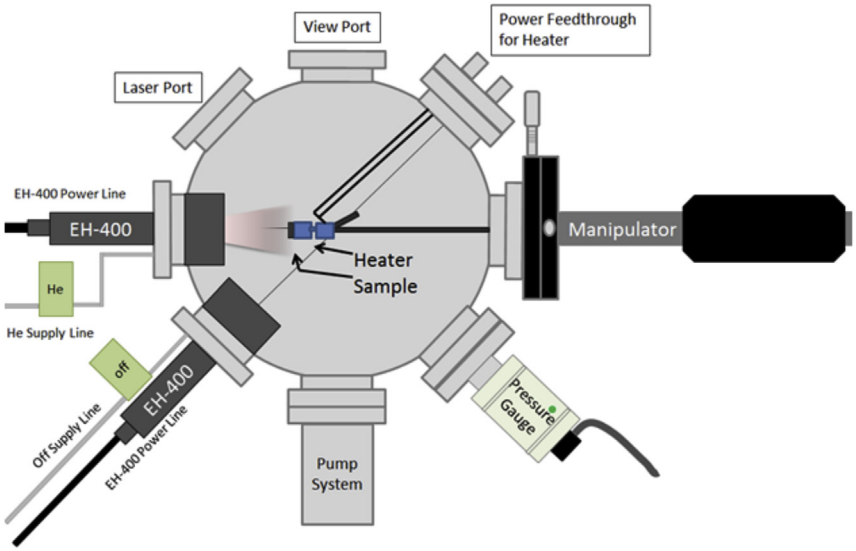

Fig. 1. Schematic diagram of the experimental set up for ion irradiation at CMUXE.

on temperature and Ta concentrations. The significant increase in surface damage observed when increasing temperature can be explained by an increase in the diffusion of small bubbles and vacancies [6,31]. This demonstrates the importance of mobility of small bubble and vacancy in bubble growth. Increased temperatures lead to increase in small bubble diffusion, vacancy diffusion, and vacancy concentration [32] all of which accelerates surface morphology evolution leading to fuzz formation as discussed in Ref. [12]. Perhaps the more interesting trend is the effect of the Ta concentration on the surface damage that appears at the 1023 K irradiation temperature. There is a noticeable difference as Ta concentration is increased even by a few wt.%. The pure W sample in Fig. 2(e) is already showing tendril growth, while the W-1Ta. W-3Ta, and W-5Ta images (Fig. 2(f) -(h)) are still clearly in the pore formation stage. There are even visual differences among the W-1Ta, the W-3Ta, and W-5Ta samples in terms of pore size and density near the surface. It seems, as if the presence of Ta (in W-Ta alloy samples) is slowing down the fuzz formation process as compared to pure W. This improvement is well aligned with the slight crystallographic changes in W due to the presence of Ta in W-Ta alloys.

The final set of SEM images is shown in Fig. 2 (i) - (l). This is a set of SEM images for four W-Ta alloy samples (W, W-1Ta, W-3Ta, and W-5Ta). Once again, in each case, samples were exposed to 100 eV He^+ ions, only this time at 1173 K. The key point to emphasize from these images is that the presence of Ta does not suppress or prevent fuzz formation. All the samples show a fuzz-like surface, indicating that the alloying of Ta with W only delays the formation of fuzz.

3.2. Optical reflectivity studies

Optical reflectivity measurements were made on selected W-Ta samples using a combination of halogen and deuterium light sources with a beam diameter of ~1 mm. These measurements are helpful in correlating surface roughness with the different morphologies observed in the SEM micrographs. Fig. 3 shows the optical reflectivity data for two different temperature cases. Fig. 3 shows the optical reflectivity data for the 873 K case, and the 1023 K case. The 1173 K samples were omitted from this figure as all the samples show fully formed fuzz and exhibit near zero reflectivity. Both 823 K and 1023 K cases show a trend of increasing reflectivity as a function of Ta concentration over all displayed wavelengths. This is in good agreement with SEM investigations which show a correlation between the presence of Ta and relatively lower surface modification. The optical reflectivity data in 823 K case shows notable differences in the surface roughness between all the samples, however the surface deterioration observed SEM studies in the same samples are very similar. This is explained by the higher sensitivity of the optical measurement technique. The optical reflectivity is less across all wavelengths, for all samples when comparing the 1023 K case to the 873 K case. This is good agreement with SEM studies, where we observed denser fuzz with increasing target temperature.

3.3. X-ray diffraction studies

X-ray diffraction was performed on selected samples to investigate the change in the crystallographic structure of W due to the presence of Ta and the respective effect it has on morphology evolution in W and W-Ta alloys. The XRD facility used in this study, is not monoenergetic. It uses a copper source with characteristic X-ray wavelengths, $K_{\alpha 1}$, $K_{\alpha 2}$ of 1.5406 and 1.5444 Å, respectively. Fig. 4 is 2θ, XRD scans of pure W and W-5Ta for four different cases: (a) Pure W Pristine (b) Pure W Irradiated (c) W-5Ta Pristine and (d) W-5Ta Irradiated. The samples irradiated at1023 K were selected for XRD analysis because the showed the greatest variation is surface damage as a function of Ta concentration. The wide XRD scans reveal BCC α-W (110), (200), (211) and (220) XRD peaks corresponding to 2θ values of 40.265, 58.274, 73.195, and 87.021, respectively (for pure W pristine) [33]. The same α-phase and diffraction patterns were observed for the W-5Ta samples; however the peak positions were slightly shifted. This is expected due to the complete miscibility of Ta in W [34]. The wide scan points to the lack of impurities which is corroborated with the XPS results discussed later. Detailed analysis of the (110) peak is shown in Fig. 5 to obtain specific information about the differences in crystallographic structure between the pure W and the W-5Ta sample before and after irradiation.

Fig. 5 shows two XRD region scans over the (110) plane peak for (a) unirradiated pure W and W-5Ta, and (b) pure tungsten and W-5Ta exposed to low energy He^+ ion irradiation at 1023 K. In both cases there is an additional XRD peak (slightly offset from the main

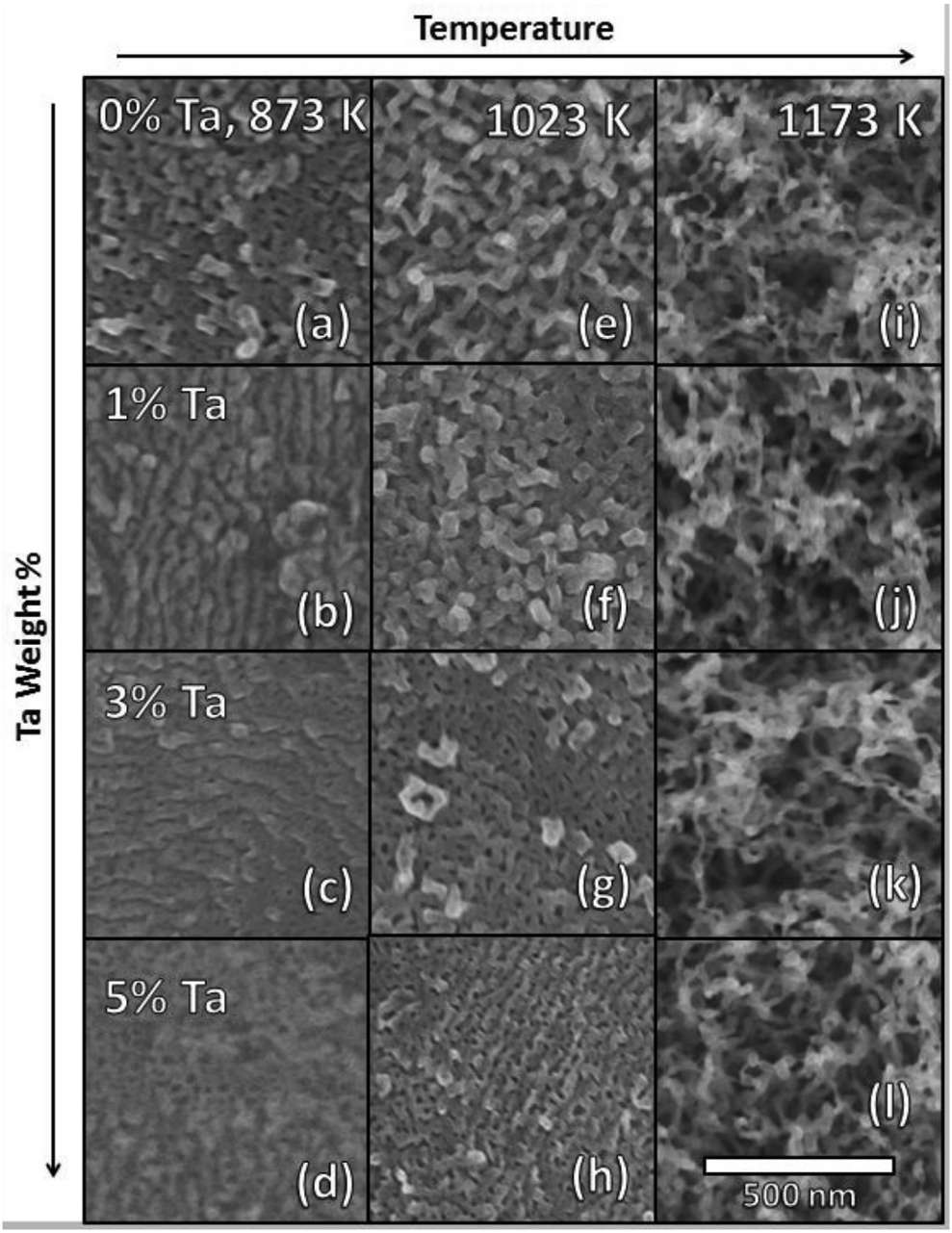

Fig. 2. SEM images of 4 W-Ta alloy samples (W, W-1TA, W-3Ta, and W-5Ta). In each case ion exposer of 100 eV, helium ions with a constant flux of 1.15×10^{21} ions m^{-2} s^{-1}, for 1 h duration at 873 (a)–(d), 1023 (e)–(h), and 1173 K (i)–(l).

XRD (110) peak). This is the (110) peak from the $K_{\alpha 2}$ X-rays. This was confirmed by using the two peak position and Bragg's Law to back out the lattice parameter alloy. By using the $K_{\alpha 1}$ wavelength for the main peak, and the $K_{\alpha 2}$ wavelength for the second peak, both peaks returned the same lattice parameter spacing. This confirms that the second peak is indeed due to the presence of $K_{\alpha 2}$ x-rays. Thus, for the subsequent analysis of peak position and shifting, only the $K_{\alpha 1}$ peak locations will be discussed.

In Fig. 5 (a) the peak position for the pure W sample is $2\theta = 40.268^{\circ}$. Applying Bragg's law, the interplaner spacing d_{hkl} can be found using the equation $d_{hkl} = \frac{n\lambda}{2 \sin \theta}$. Where, n, λ, and θ are Bragg diffraction order, X-ray wavelength, and Bragg angle, respectively. Using this relation for (110) planes and that the crystal structure is BCC, the lattice parameter spacing was found to be a = 3.165 Å. Similarly for W-5Ta sample, for $2\theta = 40.188^{\circ}$, it gives a = 3.171 Å. The reported lattice parameters for BCC W and Ta are 3.165 and 3.306 Å, respectively [35]. Ta is fully miscible in W and therefore forms a binary alloy [36]. Consequently, Vegard's law $a_{alloy} = (x_1)a_1 + x_2 a_2$ is applicable to yield a good approximation of the expected lattice parameter for W-Ta alloys [36]. Here, a_1 and a_2 correspond to the respective lattice parameters, and x is the respective weight %. Applying Vegard's law to the W-5Ta sample yields an expected lattice parameter of 3.172 Å. Both of the experimentally determined values for pure tungsten and W-5Ta match very well with what is expected from literature. It seems as if the shift to a larger average lattice parameter for this W-Ta alloy is playing a major role in the surface morphology evolution of W-Ta material which is a binary alloy with only a few weight % of Ta. This

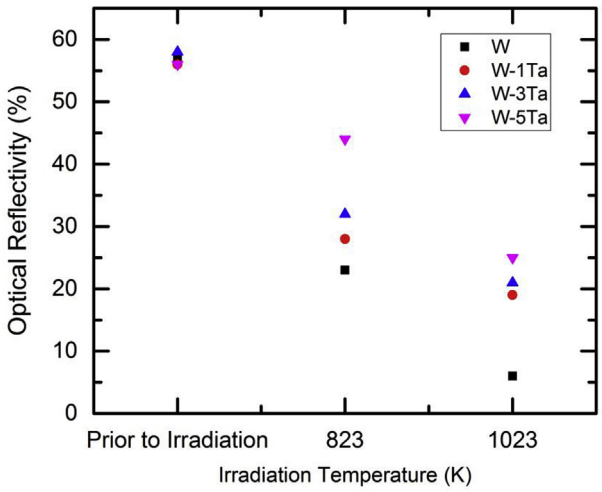

Fig. 3. Optical reflectivity values for W, W-1Ta, W-3Ta, and W-5Ta alloy samples at two temperatures 873 K and 1023 K compared to the pristine unirradiated values. Each case was exposed to 100 eV, helium ion irradiation, with a flux of 1.15×10^{21} ions m^{-2} s^{-1}, for 1 h duration. Optical reflectivity measurements were taken for 700 nm wavelength.

implies that the melting point and other thermo-mechanical properties are very near that of pure W. Therefore, it is unlikely

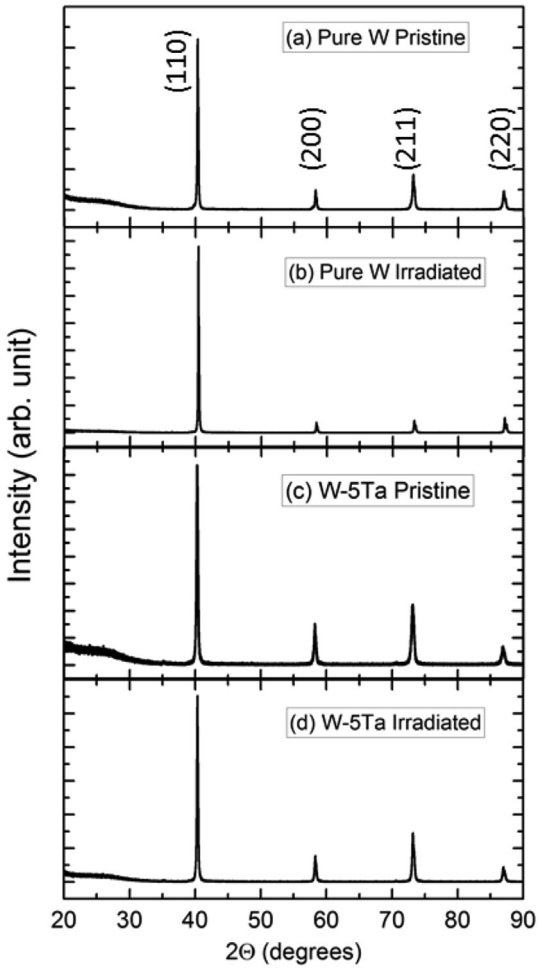

Fig. 4. Wide θ-2θ XRD scans for (a) Pure W Pristine (b) Pure W Irradiated (c) W-5Ta Pristine (d) W-5Ta Irradiated.

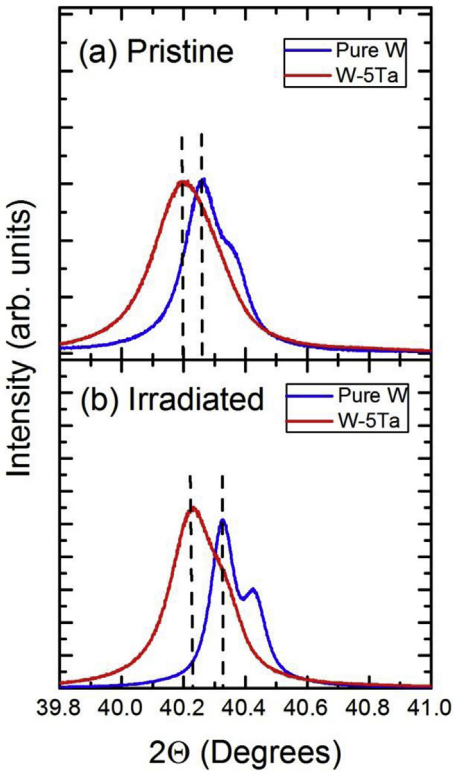

Fig. 5. High resolution XRD scans for (110) peak for (a) Pristine and (b) irradiated pure W and W-5Ta samples at 1023 K.

that these physical properties are driving the significant morphology differences observed in Fig. 2. However, larger spacing in the crystal structure may lead to more room available for the trapping of He. This in turn could lead to a larger quantity of trapped He required to induce fuzz formation. This theory also matches the fact that the increased lattice parameter does not fully prevent the fuzz as seen in Fig. 2 (i) - (l). The larger lattice parameter size simply means it takes a larger fluence of helium ions hitting the surface to reach some saturation point at which the fuzz formation processes would proceed normally as seen with traditional W samples.

Fig. 5 (b) is a similar XRD scan as in 5 (a), but on irradiated samples. Repeating the process previously discussed, the lattice parameters for pure W and W-5Ta were found to be 3.160 and 3.168 Å, respectively. These values are slightly different from the values found for the unirradiated samples. The shift to slightly smaller lattice parameters is a result of a shift to higher 2θ values. This type of shift can be caused for several reasons, but most notably it can be a result of a compressive stress on the crystal structure. The accumulation of helium bubbles in the crystal structure and grain boundaries essentially push the lattice atoms closer together. Furthermore the magnitude of the shift for the pure W sample is ~0.005 Å, while the W-5Ta shift is ~0.003 Å. This result is expected because the W-5Ta has larger average lattice spacing compared to the pure W sample. Thus, when exposed to the same He fluence there is more room for the trapped He which means that there is likely less compressive stress being applied to the lattice, which causes a smaller observed shift. Strain values, from the XRD data, for each case, for pure W pristine, pure W irradiated, W-5Ta pristine, W-Ta irradiated, have also been calculated using the method described in one of our previous report [37]. By investigating the change in the full width half max (FWHM) of the W/W-Ta XRD peaks it is possible to determine a strain value for each

sample. The observed strain values, 0.0344 (pure W pristine), 0.0288 (pure W irradiated), 0.0478 (W-5Ta pristine), and 0.0399 (W-5Ta irradiated) are in well agreement with the observed change in lattice parameters, 3.165 Å (pure W pristine), 3.160 Å (pure W irradiated), 3.171 Å (W-5Ta pristine), and 3.168 Å (W-5Ta irradiated) discussed previously.

4. Conclusion

In summary, the experiments summarized in this work discuss the low energy He^+ ion irradiations of W and W-Ta alloys in fusion relevant conditions. He^+ ion exposures were conducted at several target temperatures. SEM imaging of the samples reveal significant changes in the surface evolutions, based on Ta concentration and temperature. The low temperature exposures at 873 K showed little surface modification for all samples; nevertheless the changes in W-Ta sample with respect to pure W were notable. This is in agreement with the optical reflectivity results which show notable differences in reflectivity values among the samples, in particular relatively more surface imperfections for pure W samples as compared to W-Ta alloy samples. A similar trend was observed for 1023 K ion exposure cases as well. At 1173 K we observed fully developed fuzz structures for all the samples. This suggests that even though there might be a slight enhancement in the prevention of surface morphology evolution, the presence of Ta does not suppress the fuzz formation process. The Ta concentration seems only to push the fluence threshold for fuzz formation higher.

Extensive XRD studies provided information about the crystallographic structure of the samples and revealed a plausible correlation between the atomic spacing of the material and corresponding accumulated damage. The larger crystal lattice of the W-Ta samples required a larger fluence of helium ions hitting the surface to reach some saturation point at which point the fuzz formation processes proceeded normally as seen in the pure tungsten samples. While the performance of W-Ta alloys samples do not exhibit a complete resistance to surface modification, this work does highlight an important connection between crystal structure and damage accumulation. This may be of use in designing better PFC materials for future fusion devices.

Acknowledgment

This research was partially supported by National Science Foundation (Grant Number:1243490-OISE) under the PIRE project.

References

[1] J. Davis, V. Barabash, a Makhankov, L. Plöchl, K. Slattery, Assessment of tungsten for use in the ITER plasma facing components, J. Nucl. Mater. 258–263 (1998) 308–312, http://dx.doi.org/10.1016/S0022-3115(98)00285-2.

[2] H. Bolt, V. Barabash, G. Federici, J. Linke, A. Loarte, J. Roth, K. Sato, Plasma facing and high heat flux materials - needs for ITER and beyond, J. Nucl. Mater 307–311 (2002) 43–52, http://dx.doi.org/10.1016/S0022-3115(02)01175-3.

[3] G. Federici, a Loarte, G. Strohmayer, Assessment of erosion of the ITER divertor targets during type I ELMs, Plasma Phys. Control. Fusion 45 (2003) 1523–1547, http://dx.doi.org/10.1088/0741-3335/45/9/301.

[4] B. Lipschultz, X. Bonnin, G. Counsell, a Kallenbach, a Kukushkin, K. Krieger, a Leonard, a Loarte, R. Neu, R.a Pitts, T. Rognlien, J. Roth, C. Skinner, J.L. Terry, E. Tsitrone, D. Whyte, S. Zweben, N. Asakura, D. Coster, R. Doerner, R. Dux, G. Federici, M. Fenstermacher, W. Fundamenski, P. Ghendrih, a Herrmann, J. Hu, S. Krasheninnikov, G. Kirnev, a Kreter, V. Kurnaev, B. LaBombard, S. Lisgo, T. Nakano, N. Ohno, H.D. Pacher, J. Paley, Y. Pan, G. Pautasso, V. Philipps, V. Rohde, D. Rudakov, P. Stangeby, S. Takamura, T. Tanabe, Y. Yang, S. Zhu, Plasma–surface interaction, scrape-off layer and divertor physics: implications for ITER, Nucl. Fusion 47 (2007) 1189–1205, http://dx.doi.org/10.1088/0029-5515/47/9/016.

[5] J.N. Brooks, J.P. Allain, R.P. Doerner, a Hassanein, R. Nygren, T.D. Rognlien, D.G. Whyte, Plasma–surface interaction issues of an all-metal ITER, Nucl. Fusion 49 (2009) 35007, http://dx.doi.org/10.1088/0029-5515/49/3/035007.

[6] D. Nishijima, M.Y. Ye, N. Ohno, S. Takamura, Formation mechanism of bubbles and holes on tungsten surface with low-energy and high-flux helium plasma irradiation in NAGDIS-II, J. Nucl. Mater. 329–333 (2004) 1029–1033, http://dx.doi.org/10.1016/j.jnucmat.2004.04.129.

[7] F. Sefta, K.D. Hammond, N. Juslin, B.D. Wirth, Tungsten surface evolution by helium bubble nucleation, growth and rupture, Nucl. Fusion 53 (2013) 73015, http://dx.doi.org/10.1088/0029-5515/53/7/073015.

[8] S. Sharafat, A. Takahashi, Q. Hu, N.M. Ghoniem, A description of bubble growth and gas release of helium implanted tungsten, J. Nucl. Mater. 386–388 (2009) 900–903, http://dx.doi.org/10.1016/j.jnucmat.2008.12.318.

[9] S.B. Gilliam, S.M. Gidcumb, N.R. Parikh, D.G. Forsythe, B.K. Patnaik, J.D. Hunn, L.L. Snead, G.P. Lamaze, Retention and surface blistering of helium irradiated tungsten as a first wall material, J. Nucl. Mater 347 (2005) 289–297, http://dx.doi.org/10.1016/j.jnucmat.2005.08.017.

[10] M.Y. Ye, H. Kanehara, S. Fukuta, N. Ohno, S. Takamura, Blister formation on tungsten surface under low energy and high flux hydrogen plasma irradiation in NAGDIS-I, J. Nucl. Mater. 313–316 (2003) 72–76, http://dx.doi.org/10.1016/S0022-3115(02)01349-1.

[11] T. Venhaus, R. Causey, R. Doerner, T. Abeln, Behavior of tungsten exposed to high fluences of low energy hydrogen isotopes, J. Nucl. Mater. 290–293 (2001) 505–508, http://dx.doi.org/10.1016/S0022-3115(00)00443-8.

[12] S. Kajita, W. Sakaguchi, N. Ohno, N. Yoshida, T. Saeki, Formation process of tungsten nanostructure by the exposure to helium plasma under fusion relevant plasma conditions, Nucl. Fusion 49 (2009) 95005, http://dx.doi.org/10.1088/0029-5515/49/9/095005.

[13] M.J. Baldwin, R.P. Doerner, Formation of helium induced nanostructure “fuzz” on various tungsten grades, J. Nucl. Mater 404 (2010) 165–173, http://dx.doi.org/10.1016/j.jnucmat.2010.06.034.

[14] R.P. Doerner, M.J. Baldwin, P.C. Stangeby, An equilibrium model for tungsten fuzz in an eroding plasma environment, Nucl. Fusion 51 (2011) 43001, http://dx.doi.org/10.1088/0029-5515/51/4/043001.

[15] P.L. Raffo, Yielding and fracture in tungsten and tungsten-rhenium alloys, J. Less-Common Met. 17 (1969) 133–149, http://dx.doi.org/10.1016/0022-5088(69)90047-2.

[16] S. Wurster, B. Gludovatz, R. Pippan, High temperature fracture experiments on tungsten-rhenium alloys, Int. J. Refract. Met. Hard Mater 28 (2010) 692–697, http://dx.doi.org/10.1016/j.ijrmhm.2010.03.002.

[17] I. Wesemann, W. Spielmann, P. Heel, A. Hoffmann, Fracture strength and microstructure of ODS tungsten alloys, Int. J. Refract. Met. Hard Mater 28 (2010) 687–691, http://dx.doi.org/10.1016/j.ijrmhm.2010.05.009.

[18] K.H. Lee, S.I. Cha, H.J. Ryu, M.F. Dilmore, S.H. Hong, Effect of mechanical alloying process on microstructure and mechanical properties of ODS tungsten heavy alloys, J. Alloys Compd. 434–435 (2007) 433–436, http://dx.doi.org/10.1016/j.jallcom.2006.08.284.

[19] A. Alamo, J.L. Bertin, V.K. Shamardin, P. Wident, Mechanical properties of 9Cr martensitic steels and ODS-FeCr alloys after neutron irradiation at 325 °C up to 42 dpa, J. Nucl. Mater. 367–370 A (2007) 54–59, http://dx.doi.org/10.1016/j.jnucmat.2007.03.166.

[20] N. Akasaka, S. Yamashita, T. Yoshitake, S. Ukai, A. Kimura, Microstructural changes of neutron irradiated ODS ferritic and martensitic steels, J. Nucl. Mater. 329–333 (2004) 1053–1056, http://dx.doi.org/10.1016/j.jnucmat.2004.04.133.

[21] S. Wurster, B. Gludovatz, A. Hoffmann, R. Pippan, Fracture behaviour of tungsten-vanadium and tungsten-tantalum alloys and composites, J. Nucl. Mater 413 (2011) 166–176, http://dx.doi.org/10.1016/j.jnucmat.2011.04.025.

[22] D.E.J. Armstrong, A.J. Wilkinson, S.G. Roberts, Mechanical properties of ion-implanted tungsten–5 wt% tantalum, Phys. Scr. T145 (2011) 14076, http://dx.doi.org/10.1088/0031-8949/2011/T145/014076.

[23] M. Wirtz, J. Linke, G. Pintsuk, L. Singheiser, I. Uytdenhouwen, Comparison of the thermal shock performance of different tungsten grades and the influence of microstructure on the damage behaviour, Phys. Scr. T145 (2011) 14058, http://dx.doi.org/10.1088/0031-8949/2011/T145/014058.

[24] J. Linke, T. Loewenhoff, V. Massaut, G. Pintsuk, G. Ritz, M. Rödig, a Schmidt, C. Thomser, I. Uytdenhouwen, V. Vasechko, M. Wirtz, Performance of different tungsten grades under transient thermal loads, Nucl. Fusion 51 (2011) 73017, http://dx.doi.org/10.1088/0029-5515/51/7/073017.

[25] Y. Zayachuk, M.H.J. 't Hoen, P.A.Z. van Emmichoven, D. Terentyev, I. Uytdenhouwen, G. van Oost, Y. Zayachuk, Surface modification of tungsten and tungsten–tantalum alloys exposed to high-flux deuterium plasma and its impact on deuterium retention, Nucl. Fusion 53 (2013).

[26] Y. Zayachuk, M.H.J. 't Hoen, P.a Zeijlmans van Emmichoven, I. Uytdenhouwen, G. van Oost, Deuterium retention in tungsten and tungsten–tantalum alloys exposed to high-flux deuterium plasmas, Nucl. Fusion 52 (2012) 103021, http://dx.doi.org/10.1088/0029-5515/52/10/103021.

[27] Y. Zayachuk, A. Manhard, M.H.J. 'T Hoen, W. Jacob, P.A. Zeijlmans Van Emmichoven, G. Van Oost, The effect of ion flux on plasma-induced modification and deuterium retention in tungsten and tungsten-tantalum alloys, J. Nucl. Mater 464 (2015) 69–72, http://dx.doi.org/10.1016/j.jnucmat.2015.04.028.

[28] J.K. Tripathi, S.S. Harilal, a Hassanein, Low energy Ar + ion irradiation induced surface modification in cadmium zinc telluride (CdZnTe), Mater. Res. Express 1 (2014) 35904, http://dx.doi.org/10.1088/2053-1591/1/3/035904.

[29] J.K. Tripathi, T.J. Novakowski, S. Gonderman, N. Bharadwaj, A. Hassanein, The effect of carbon impurities on molybdenum surface morphology evolution under high-flux low-energy helium ion irradiation, J. Nucl. Mater 478 (2016)

287–294, http://dx.doi.org/10.1016/j.jnucmat.2016.06.026.
[30] N. Fairley, CasaXPS: processing software for XPS, AES, SIMS and more, 2016. http://www.casaxps.com (Date of access: 09/20/2016).
[31] N. Marochov, L.J. Perryman, P.J. Goodhew, Growth of inert gas bubbles after implantation, J. Nucl. Mater 149 (1987) 296–301.
[32] H. Ullmaier, Review paper the influence of helium on the bulk properties of fusion reactor, Nucl. Fusion. 24 (1984) 1039. http://iopscience.iop.org/0029-5515/24/8/009.
[33] W.B. Pearson, A Handbook of Lattice Spacings and Structures of Metals and Alloys: International Series of Monographs on Metal Physics and Physical Metallurgy, vol. 4, Elsevier, 2013.
[34] Handbook, Alloy Phase Diagrams 3 (1990) 1453.
[35] E. Lassner, W.-D. Schubert, Tungsten: Properties, Chemistry, Technology of the Element, Alloys, and Chemical Compounds, Springer Science & Business Media, 2012.
[36] V.A. Lubarda, On the effective lattice parameter of binary alloys, Mech. Mater 35 (2003) 53–68, http://dx.doi.org/10.1016/S0167-6636(02)00196-5.
[37] P.C. Srivastava, J.K. Tripathi, Giant magnetoresistance (GMR) in swift heavy ion irradiated Fe films on c-silicon (Fe/c-Si), J. Phys. D. Appl. Phys. 39 (2006) 1465–1471, http://dx.doi.org/10.1088/0022-3727/39/8/001.